VPS35 promotes cell proliferation via EGFR recycling and enhances EGFR inhibitors response in gastric cancer

Junxian Yu,[a,b,c] Haoran Feng,[a,b,c] Qingqing Sang,[a,b,c] Fangyuan Li,[a,b] Mengdi Chen,[a,b] Beiqin Yu,[a,b] Zhuoqing Xu,[a,b] Tao Pan,[a,b] Xiongyan Wu,[a,b] Junyi Hou,[a,b] Zhenggang Zhu,[a,b] Chao Yan,[a,b] Liping Su,[a,b] Jianfang Li,[a,b,**] and Bingya Liu[a,b,*]

[a]Department of General Surgery, Ruijin Hospital, Shanghai Jiao Tong University School of Medicine, Shanghai 200025, People's Republic of China
[b]Shanghai Key Laboratory of Gastric Neoplasms, Shanghai Institute of Digestive Surgery, Ruijin Hospital, Shanghai Jiao Tong University School of Medicine, Shanghai 200025, People's Republic of China

eBioMedicine
2023;89: 104451
Published Online xxx
https://doi.org/10.1016/j.ebiom.2023.104451

Summary

Background Vacuolar protein sorting-associated protein 35 (VPS35) is a core component of the retromer complex which mediates intracellular protein transport. It is well known that dysfunctional VPS35 functions in the accumulation of pathogenic proteins. In our previous study, VPS35 was found to be a potential gene related to poor prognosis in gastric cancer. However, the biological functions of VPS35 in gastric cancer remain unclear.

Methods Cell viability assays were performed to examine whether VPS35 affected cell proliferation. Immunoprecipitation and biotin assays showed that VPS35 bound to epidermal growth factor receptor (EGFR) in the cytoplasm and recycled it to the cell surface. Patient-derived xenografts and organoids were used to evaluate the effect of VPS35 on the response of gastric cancer to EGFR inhibitors.

Findings VPS35 expression levels were upregulated in tumour tissues and correlated with local tumour invasion and poor survival in patients with gastric cancer. VPS35 promoted cell proliferation and increased tumour growth. Mechanistically, VPS35 selectively bound to endocytosed EGFR in early endosomes and recycled it back to the cell surface, leading to the downstream activation of the ERK1/2 pathway. We also found that high VPS35 expression levels increased the sensitivity of the xenograft and organoid models to EGFR inhibitors.

Interpretation VPS35 promotes cell proliferation by recycling EGFR to the cell surface, amplifying the network of receptor trafficking. VPS35 expression levels are positively correlated with gastric cancer sensitivity to EGFR inhibitors, which offers a potential method to stratify patients for EGFR inhibitor utilisation.

Funding National Natural Science Foundation of China.

Keywords: VPS35; Retromer; EGFR; Erlotinib; Gastric cancer

Introduction

Gastric cancer ranks fifth in terms of cancer incidence and fourth among the leading causes of death in the world.[1,2] The Cancer Genome Atlas (TCGA) Network has depicted a huge landscape of major genetic aberrations in gastric cancer[3]; however, the translation of molecular characterisation into clinical drug application needs further exploration.[4] An important goal is to delineate the genomic regulation network and determine vital genes for cell survival, which can be recognized using the genome-scale CRISPR-Cas9 screening method.[5] In our previous study, we constructed a gastric cancer prognosis model based on a functional genome database generated from CRISPR-Cas9 screen. Among the constituents of this model, vacuolar protein sorting-associated protein 35 (VPS35), with a hazard ratio of ~2,[6] attracted our attention.

VPS35 plays a predominant role in cargo selection of the retromer complex,[7] which is well known as a retrograde transporter, trafficking proteins from endosomes to the trans-Golgi network (TGN).[8] Retromers can also prevent the missorting of selected transmembrane cargo

*Corresponding author. Department of General Surgery, Shanghai Key Laboratory of Gastric Neoplasms, Shanghai Institute of Digestive Surgery, Ruijin Hospital, Shanghai Jiao Tong University School of Medicine, Shanghai, 200025, People's Republic of China.
**Corresponding author. Department of General Surgery, Shanghai Key Laboratory of Gastric Neoplasms, Shanghai Institute of Digestive Surgery, Ruijin Hospital, Shanghai Jiao Tong University School of Medicine, Shanghai, 200025, People's Republic of China.
E-mail addresses: liubingya@sjtu.edu.cn (B. Liu), ljf40349@rjh.com.cn (J. Li).
[c]These authors contributed equally to this work.

Research in context

Evidence before this study

The retromer complex mediates protein transport from endosomes to other intracellular compartments. Vacuolar protein sorting-associated protein 35 (VPS35) is a core component of retromer complex in cargo sorting. It is well illustrated that dysfunctional VPS35 participates in the accumulation of pathogenic proteins in Parkinson's disease. Although several studies have proposed VPS35 correlated to poor prognosis in cancer, the underlying mechanisms of VPS35 function in cancer remain unclear.

Added value of this study

VPS35 was found to promote gastric cancer by recycling EGFR to the cell surface and activating downstream pathways. By increasing the density of EGFR on the cell surface, VPS35 enhanced gastric cancer sensitivity to EGFR inhibitors.

Implications of all the available evidence

This study increases our knowledge of the intracellular protein transportation and receptor trafficking network. These findings indicate that VPS35 is a potential treatment effect marker to stratify gastric cancer patients for anti-EGFR therapy.

proteins into the lysosomal degradation pathway.[9] The retromer complex consists of three main components: VPS35, VPS26, and VPS29.[7] In addition to its canonical function in endosome-to-TGN transportation, VPS35 has also been found to participate in endocytosed protein-tetherin transportation to the cell surface.[10] Many studies have focused on VPS35 mutants which cause transportation imbalances and pathogenic protein (α-synuclein) accumulation in Parkinson's disease.[9] Our previous study showed that VPS35 is a prognosis-related gene in gastric cancer.[6] However, the carcinogenic mechanism of protein transport via VPS35 was still unclear.[11]

In gastric cancer, many oncogenic drivers have been identified from TCGA database, including human epidermal factor receptor 2 (HER2), epidermal growth factor receptor (EGFR), and fibroblast growth factor receptor 2 (FGFR2).[12] EGFR is a transmembrane glycoprotein and member of the receptor tyrosine kinase ErbB family.[13] Upon binding to its ligands (EGF, amphiregulin, and epiregulin), EGFR is endocytosed and then degraded or recycled.[14] Evidence has indicated that EGFR amplification, gain-of-function mutations, and trafficking result in proto-oncogenic events.[14–16] Whether VPS35 mediates EGFR trafficking and promotes cancer development has not been reported.

In this study, we demonstrated that VPS35 promotes cell proliferation and increases tumour growth in gastric cancer. VPS35 overexpression increased cellular EGF-saturated concentrations and increased EGFR density on the cell surface by binding to EGFR and recycling it to the cell surface. Additionally, our study sheds new light on the role of VPS35 in gastric cancer sensitivity to EGFR inhibitors, which offers a potential path to guide anti-EGFR therapy.

Methods

Specimens and ethics

All procedures of human and mouse experiments were approved by Ethics Committee of Shanghai Ruijin Hospital, Shanghai Jiao Tong University School of Medicine, Shanghai, China (Approval No.2017-6). All samples were obtained with the patients' informed consent. Excluding unpaired tumor-normal samples and samples of incomplete clinical information, specimens of tumour and adjacent non-tumour tissues from 96 gastric cancer patients with intact clinical information who underwent D2 gastrectomy were collected. Patients who underwent preoperative treatment such as radiation or chemotherapy were excluded from our study.

Antibodies and reagents

The antibodies to VPS35 (ab157220, RRID: AB_2636885), EGFR (ab52894, RRID: AB_869579), CyclinD1 (ab134175, RRID: AB_2750906), CDK2 (ab32147, RRID: AB_726775), phospho-CDK2 (ab68265, RRID: AB_1139872), AKT1 (ab108202, RRID: AB_10860681), phospho-AKT1 (ab81283, RRID: AB_2224551), and Ki-67(ab16667, RRID: AB_302459) were purchased from Abcam (Boston, MA, USA). The antibodies to ERK1/2 (4695S, RRID: AB_390779), phospho-ERK1/2 (4370T, RRID: AB_2315112), and VPS35 (81453S) were purchased from Cell Signaling Technology (Danvers, MA, USA). The antibodies to β-tubulin (10094-1-AP, RRID: AB_2210695) and GAPDH (60004-1-Ig, RRID: AB_2107436) were purchased from Proteintech (Rosemont, IL, USA).

Recombinant human EGF protein (HY-P7109), cycloheximide (HY-12320) and cetuximab (HY-P9905) were purchased from MedChemExpress (NJ, USA). BeyoClickTM EdU cell proliferation Kit with Alexa Fluor-594 (C0078S) was obtained from Beyotime (Shanghai, China). The Cell Cycle Staining Kit was purchased from BD Biosciences (New Jersey, USA).

Cell culture

Human gastric cancer cells AGS (RRID:CVCL_0139) and NCI-N87 (RRID:CVCL_1603) were purchased from American Type Culture Collection (ATCC, USA), and MGC803 (RRID:CVCL_5334), MKN28 (RRID:CVCL_1416), MKN45 (RRID:CVCL_0434), HGC27 (RRID:CVCL_1279) and HS-746T (RRID:CVCL_0333) cells were purchased from Shanghai Institutes for Biological Sciences, Chinese Academy of Sciences. Cells were authenticated by STR profiling and free of

mycoplasma contamination. Cells were cultured as previously described.[6]

Lentivirus vectors and infection

For knockdown of VPS35, target shRNA sequences were subcloned into GPH-shRNA Lentivector (CMV-copGFP-T2A-puro-H1-MCS) (Bioegene, Shanghai, China). The shRNA of VPS35 targeted the following sequence: 5′-CC TCCAGACTTTGAATCCTTT-3′. The shRNA of EGFR targeted the following sequence: 5′-GTGGCTGGTTA TGTCCTCATT-3′. Human full-length cDNA of VPS35 was subcloned into pGMLV-CMV-MCS-EF1-T2A-Blasticidin lentivirus vector (Genomeditech, Shanghai, China). The transfection process and cell selection were performed as previously described.[6]

Cell viability, colony formation assay and cell cycle analysis

Cell viability, colony formation assay and cell cycle analysis were performed as previously described.[6] Cell viability assay was evaluated with the Cell counting Kit-8 (CCK8, Dojindo Molecular Technologies, Kumamoto, Japan) according to the manufacturer's protocol.

BeyoClickTM EdU cell proliferation assay

Cells were cultured in 24-well plates. EdU was added to the culture medium and the assay was completed according to the manufacturer's protocol.

Western blotting

Western blotting was performed as previously described.[6]

RNA extraction and quantitative real-time PCR (qRT-PCR)

RNA extraction and qRT-PCR were performed as previously described.[6] The sequences of the primers were as follows: GAPDH, forward, 5′-GCACCGTCAAGGC TGAGAAC, reverse, 5′-ATGGTGGTGAAGACGCCAGT; VPS35, forward, 5′-GTTTTGACTGGCATATTGGAGCA, reverse, 5′-TCTGGTGTAACTCAGCACAGG. The expression level was normalized to the internal control and determined by a 2-ΔΔCT method.

Library construction and RNA-Seq

Total RNA was extracted from the tissue using TRIzol® Reagent according the manufacturer's instructions (Invitrogen) and genomic DNA was removed using DNase I (TaKara). Then RNA quality was determined by 2100 Bioanalyser (Agilent) and quantified using the ND-2000 (NanoDrop Technologies). Only high-quality RNA sample (OD260/280=1.8~2.2, OD260/230≥2.0, RIN≥6.5, 28S:18S≥1.0, >1 μg) was used to construct sequencing library. RNA-seq transcriptome library was prepared using TruSeqTM RNA sample preparation Kit from Illumina (San Diego, CA), SuperScript double-stranded cDNA synthesis kit (Invitrogen, CA) and Phusion DNA polymerase (NEB) according to manufacturer's protocol. After quantified by TBS380, paired-end RNA-seq sequencing library was sequenced with the NovaSeq 6000 sequencer (2 × 150bp read length).

Transcriptome analysis using reference genome-based reads mapping

The raw paired end reads were trimmed and quality controlled by SeqPrep and Sickle with default parameters. Then clean reads were separately aligned to reference genome with orientation mode using HISAT2 software.[17] The mapped reads of each sample were assembled by StringTie in a reference-based approach.[18] To identify DEGs (differential expression genes), the expression level of each transcript was calculated according to the transcripts per million reads (TPM) method. RSEM[19] was used to quantify gene abundances. Essentially, differential expression analysis was performed using the DESeq2,[20] DEGs with |log2FC|>1 and Q value ≤ 0.05 were considered to be significantly different expressed. In addition, functional-enrichment analysis including GO and KEGG were performed at Bonferroni-corrected P-value ≤0.05 by Goatools and KOBAS.[21]

Immunoprecipitation and mass spectrometry (IP-MS)

IP-MS was performed as previously described.[6] Immunoprecipitation was performed using Pierce Co-Immunoprecipitation (Co-IP) Kit (88804, Thermo Fisher) according to manufacturer's protocol. ProteinChip Gold Array (Bio-Rad) with a Bio-Rad Protein Chip System Series 4000 mass spectrometer was used for analysis.

Immunofluorescence (IF) assay of EGFR degradation

Immunofluorescence assay was performed as previously described.[22,23] In brief, cells were starved overnight and stimulated with 100 ng/mL EGF and 100 μg/mL cycloheximide for indicated times. Then, cells were fixed and stained with antibodies. Images were captured using an inverted fluorescent microscope (Fluoview FV1000, Olympus). Fluorescence intensity were quantified using ImageJ as described previously.[24]

Flow cytometry

To detect the protein density on the cell membrane, flow cytometry was performed as previously described.[25] The antibodies used were APC anti-human EGFR (352905, RRID: AB_11148943, BioLegend, San Diego, CA, USA), APC anti-human CD340 (324407, RRID: AB_756123, BioLegend), APC anti-human VEGFR2 (359915, RRID: AB_2565927, BioLegend), c-MET (8198, RRID: AB_10858224, Cell Signaling Technology, Danvers, MA, USA), and Alexa Fluor® 647 donkey anti-rabbit IgG (ab150075, RRID: AB_2752244, Abcam, Boston, MA, USA).

Cell surface biotinylation assay

A modified protocol by Nishimura and Sasaki was used to examine the recycling of EGFR to the cell surface.[26] Briefly, proteins on the cell surface were marked using EZ-Link Sulfo–NHS–SS-Biotin (A39258, Thermo Fisher Scientific, Waltham, MA, USA) on ice. The cells were incubated with 100 ng/mL EGF at 37 °C for 30 min to internalise the receptors. After internalisation, cells were washed with MESNA (Thermo Fisher Scientific) for the first time to remove extra biotin. Next, cells were incubated at 37 °C for the indicated times and stripped using MESNA on ice for the second time to remove biotin linked to the recycled receptors on the cell surface. Recycling measurements have been described previously.[22,27]

H&E analysis and immunohistochemistry (IHC)

Immunohistochemistry assay was performed as previously described according to the manufacturer's protocol (Immunostain SP kit, DakoCytomation, USA).[22,23] The IHC staining scores were determined according to semi-quantitative immunoreactivity scoring (IRS) system.[28,29]

Bioinformatic analysis on GDSC, CCLE, and TCGA screens

The sensitivity of gastric cancer cell lines to erlotinib was compared using Genomics of Drug Sensitivity in Cancer (GDSC). Three sensitive and three insensitive cell lines were selected, and their gene expression data were collected from the Cancer Cell Line Encyclopedia (CCLE). Differentially expressed genes (DEGs) were analysed using the limma package. The correlation between VPS35 and each receptor was analysed using the corrplot package and GEPIA.

Dose-effect curves

Cells were plated into 96-well plates. Medium with erlotinib at concentrations of 0, 10, 20, 40, 80, 160, 320 nM was added to wells and medium was replaced every day with fresh medium with erlotinib. After 10 days culture, CCK-8 kit was used according to the manufacture's instruction.

Cell-derived and patient-derived xenograft (PDX) tumour models

BALB/c male nude mice (RRID: IMSR_JCL:JCL:mID-0001, 4–6 weeks old, purchased from SPF (Beijing) Biotechnology Co., Ltd., Beijing, China) were housed in specific pathogen-free cages and used to construct xenograft models. Animal experiments were performed in accordance with the institution's guidelines and animal research principles, and daily care has been provided. After acclimatization for 3 days in an approved facility (water and food at libitum and controlled environmental conditions), experiments were conducted. The single blind method was adopted in our experiments. Nude mice were randomised into four treatment groups (n = 5): MKN28/Ctrl, MKN28/shVPS35, HGC27/Ctrl, and HGC27/VPS35. Approximately 5×10^6 cells suspended in PBS were injected subcutaneously.

PDXs were established with tumors of gastric cancer patients from Ruijin Hospital as described previously.[30,31] For PDX transplantation, tumor fragments of 1–2 mm were subcutaneously engrafted into nude mice under anaesthesia. When tumors reached a volume of 100 mm^3, the mice were separated into 2 groups for treatment with Erlotinib (50 mg/kg, orally) or Vehicle (n = 3). Treatment was administered by gavage 5 days a week for 3 weeks. Nude mice received subcutaneous injection inoculation with 5×10^6 cells of HGC27/Ctrl and HGC27/VPS35, and were randomised into the following four treatment groups (n = 5): Ctrl-Vehicle, VPS35-Vehicle, Ctrl-Erlotinib (20 mg/kg, peritumoural injection every 2 days), and VPS35-Erlotinib. Tumour volumes were measured using calipers every 4 or 5 days and calculated with the formula: volume (mm^3) = length × width × width/2. If volumes were over 4000 mm^3 or the diameter in either dimension was greater than 20 mm (humane endpoint), mice were euthanised. Otherwise, mice were euthanised under anaesthesia after whole treatment, and tumours were removed and weighed.

Establishment and culture of patient derived organoids (PDO) from gastric cancer patients

PDO establishment was performed as previously described.[6] The tumor tissues from gastric cancer patients were digested with shaking and filtered through a 70 μm cell strainer (BD Biosciences). After centrifuged, Matrigel was added to the pellet and plated in the 24-well plate. The shVPS35 lentivirus, pGMLV-VPS35, and control lentivirus were transfected into organoids. Erlotinib were added and refreshed every day for ten days and CellTiter-Lumi™ Luminescent Cell Viability Assay Kit (Beyotime) was used to evaluate the viability.

Statistical analysis

All statistical calculations were performed using GraphPad Prism (version 8.0). Student's t tests (two-tailed) were applied to assess the statistical significance of the qPCR, gene expression, colony formation and EdU assay. Two-way ANOVA was applied on CCK-8 assays examining cell viability. Comparisons among multiple groups were analysed by the one-way ANOVA. All results were presented as the mean ± standard deviation (SD) from triplicate experiments. Chi-square

tests were performed to assess clinical and biological variables between patient groups. Log-rank analysis was used for survival analysis. Differences with P value less than 0.05 were considered statistically significant.

Role of funders

The funders had no role in the study design, data collection and analysis, decision to publish, or preparation of the manuscript.

Results

VPS35 expression was upregulated in tumour tissues of gastric cancer and indicated poor prognosis

Our previous study showed that VPS35 is closely related to the survival of gastric cancer patients.[6] To further investigate the function of VPS35 in cancer, VPS35 expression levels in tumour and adjacent non-tumour tissues were analysed in digestive system cancers

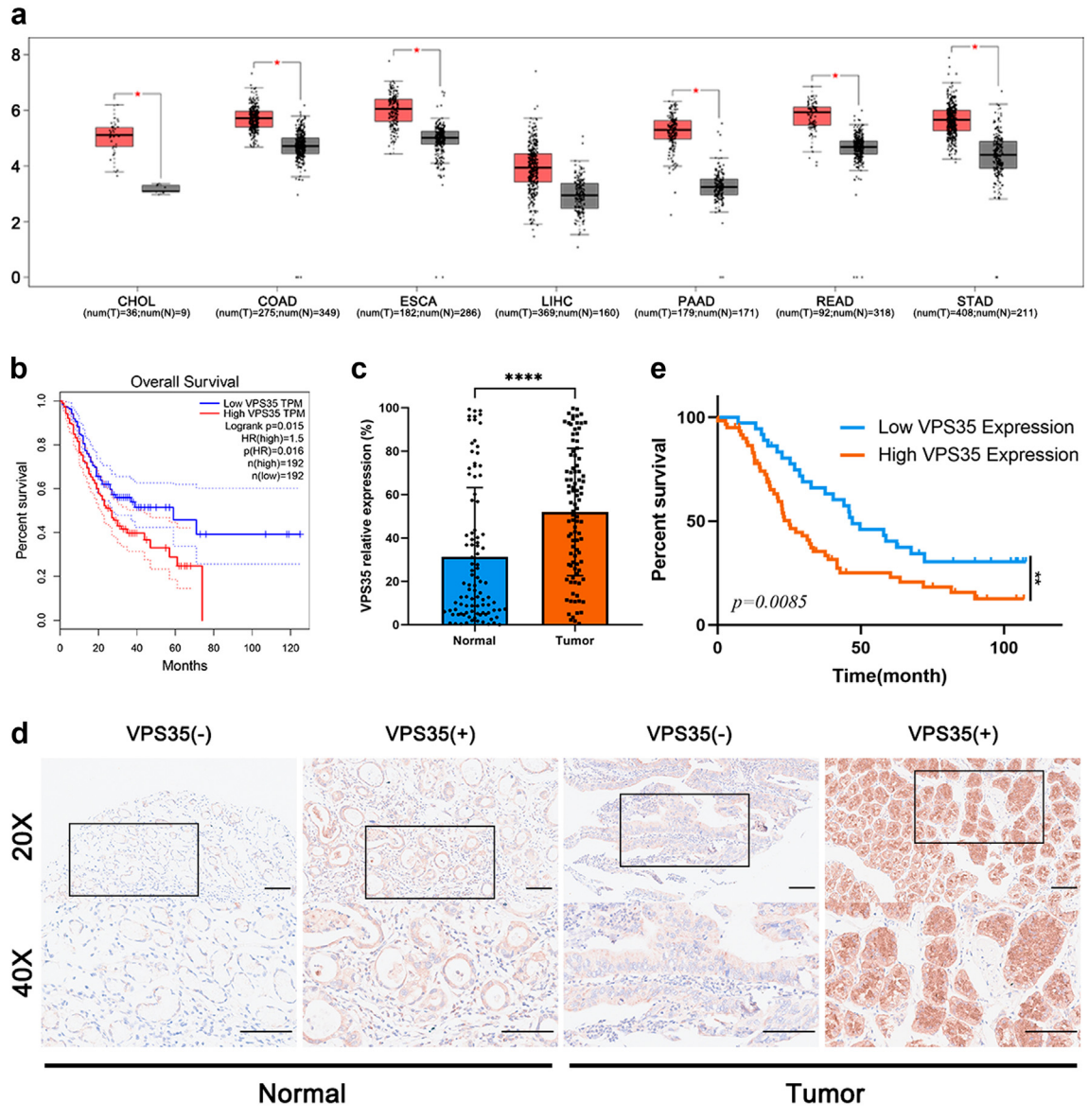

Fig. 1: **VPS35 expression upregulated in tumour tissues and associated with poor prognosis of the patients with gastric cancer.** (a) Upregulation of VPS35 in six digestive system cancer types in the GEPIA database. (b) Overall survival curves of the 384 patients in the gastric cancer cohort in GEPIA, with patients stratified based on VPS35 expression levels (Log-rank test). (c) Average immunohistochemistry (IHC) scores of VPS35 of patient samples in the Ruijin gastric cancer cohort (n = 96, Chi-square test). (d) Representative images of VPS35 IHC in gastric cancer and matched normal tissues from the Ruijin cohort. (e) Overall survival curves of our patient cohort, with patients stratified based on VPS35 expression levels (Log-rank test). (Scale bars: 100 μm, *, $p < 0.05$; **, $p < 0.01$; ***, $p < 0.001$ and ****, $p < 0.0001$.).

Clinicopathologic parameters	Number of cases N = 96	VPS 35 IHC		p-value
		Negative (36)	Positive (60)	
Age(years)				0.3998
≤60	47	20	27	
>60	49	16	33	
Sex				0.6636
Male	60	24	36	
Female	36	12	24	
Local invasion				<0.0001
T1, T2	31	24	7	
T3, T4	65	12	53	
Lymph node metastasis				0.0003
No	31	20	11	
Yes	65	16	49	
Distant metastasis				0.4248
No	78	31	47	
Yes	18	5	13	
TNM stage				0.0101
I, II	55	27	28	
III, IV	41	9	32	

Table 1: **Correlation between the Clinicopathologic features and expression of VPS35.**

based on TCGA database using GEPIA (http://gepia.cancer-pku.cn/). We found that VPS35 was upregulated in tumour tissues compared to that in the paired normal tissues in gastric, colorectal, and pancreatic cancers (Fig. 1a). Survival analysis showed that high VPS35 expression levels in tumour tissues were positively related to short survival time of patients ($p = 0.015$, Log-rank test) (Fig. 1b) in TCGA database. IHC staining of gastric cancer tissue in the cohort ($n = 96$) also showed that VPS35 protein expression in tumour tissues was higher than that in adjacent non-tumour tissues (Fig. 1c and d). Importantly, higher VPS35 staining scores were associated with deeper local invasion ($p < 0.0001$, Chi-square test), local lymph node metastasis ($p = 0.0003$, Chi-square test), and later TNM staging ($p = 0.0101$, Chi-square test) (Table 1). Patients with higher VPS35 expression in tumour tissues were correlated with shorter 5-year overall survival (OS) compared to patients with VPS35 lower-expressing tumours ($p = 0.0085$, Log-rank (Mantel–Cox) test) (Fig. 1e), consistent with the results of TCGA analysis.

VPS35 promoted gastric cancer cell proliferation *in vitro* and *in vivo*

To explore the impact of VPS35 on the proliferation of gastric cancer cells, we constructed VPS35 knockdown cells (AGS/shVPS35 and MKN28/shVPS35) by transducing shRNA, and VPS35 overexpressed cells (HGC27/VPS35 and HS-746T/VPS35) by transfecting VPS35 expression vectors (Fig. 2a and S1). Compared to the negative control cells (AGS/Ctrl, MKN28/Ctrl, HGC27/Ctrl, and HS-746T/Ctrl), VPS35 knockdown (AGS/shVPS35 and MKN28/shVPS35) significantly inhibited cell proliferation, whereas VPS35 overexpression (HGC27/VPS35 and HS-746T/VPS35) promoted the proliferation of gastric cancer cells (Fig. 2b and c). Furthermore, EdU staining also showed that VPS35 high-expressing cells were more likely to be EdU-positive than VPS35 low-expressing cells (Fig. 2d). The cell cycle assay revealed a remarkably reduced fraction of cells in the S phase and an elevated fraction of cells in the G1 phase in the AGS/shVPS35 and MKN28/shVPS35 cells. In contrast, VPS35 overexpression reversed this effect and promoted G1/S transition (Fig. 2e and f). The levels of both p-CDK2 and cyclin D (key proteins of the G1/S cell-cycle checkpoint) were dramatically decreased in AGS/shVPS35 and MKN28/shVPS35 cells, whereas CDK2 levels were stable (Fig. 2e). In contrast, HGC27/VPS35 and HS-746T/VPS35 cells exhibited increased levels of p-CDK2 and cyclin D (Fig. 2e). These findings indicate that VPS35 could accelerate cell cycle progression and promote cell proliferation in gastric cancer by activating the CDK2 and cyclin D pathways.

Given the findings described above, we further investigated the effect of VPS35 *in vivo* using xenograft tumour models. MKN28/Ctrl, MKN28/shVPS35, HGC27/Ctrl, and HGC27/VPS35 cells were inoculated subcutaneously into the flank of nude mice (Fig. 3a). After 28 days, we found that tumour weights in the MKN28/shVPS35 group were significantly lower ($p < 0.0001$, the student's t tests) than those in the MKN28/Ctrl group (Fig. 3a–b). In contrast, tumours derived from HGC27/VPS35 cells grew faster ($p < 0.0001$, the student's t tests) and weighed more ($p < 0.0001$, the student's t tests) than tumours from the HGC27/Ctrl group (Fig. 3a–b). IHC also showed that HGC27/VPS35 tumours had more p-CDK2-positive cells than HGC27/Ctrl tumours (Fig. 3c), whereas MKN28/shVPS35 tumours had more p-CDK2-negative cells than MKN28/Ctrl tumours (Fig. 3c).

Identification of VPS35 binding to EGFR

As a core component of the retromer, VPS35 binds to many proteins in endosomes to exert its function in gastric cancer. To determine which proteins VPS35 binds to, and the mechanism of its proliferation-promoting function, transcriptome profiling (RNA-Seq) was performed in MKN28/Ctrl and MKN28/shVPS35 cells (Fig. S2a). According to the gene ontology (GO) enrichment analysis of DEGs, receptor ligand activity, genes related to EGFR binding, and regulation of epithelial cell proliferation were enriched (Fig. 4a and S2b). The Kyoto Encyclopedia of Genes and Genomes (KEGG) enrichment analysis of differentially expressed genes (DEGs) indicated that genes in the MAPK signalling pathway (q-

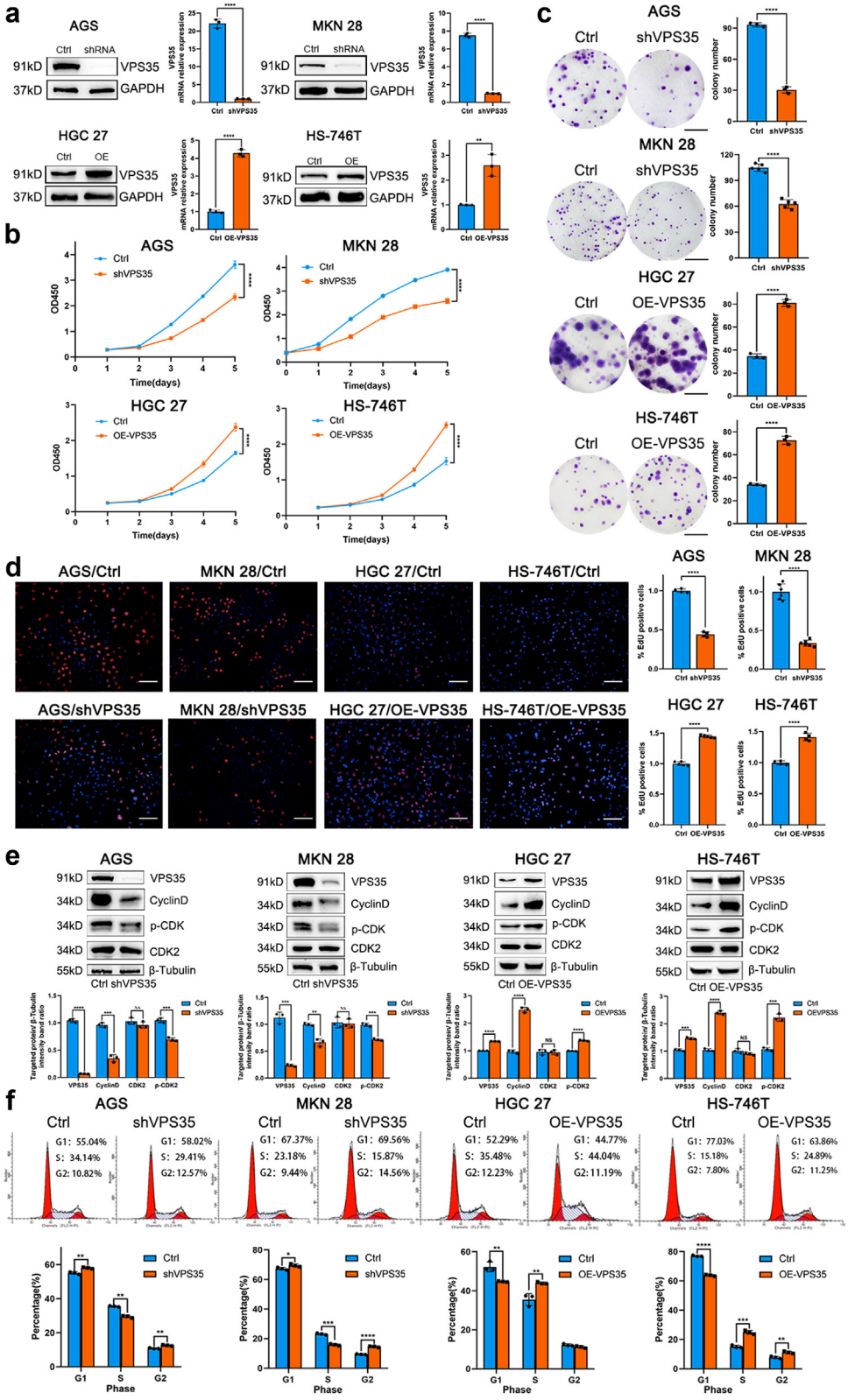

***Fig. 2:* VPS35 stimulated cell proliferation of gastric cancer in vitro.** (a) VPS35 expression knockdown by shRNA in AGS (upper left) and MKN 28 (upper right) and VPS35 overexpression in HGC 27 (lower left) and HS-746T (lower right), detected by western blotting and quantitative

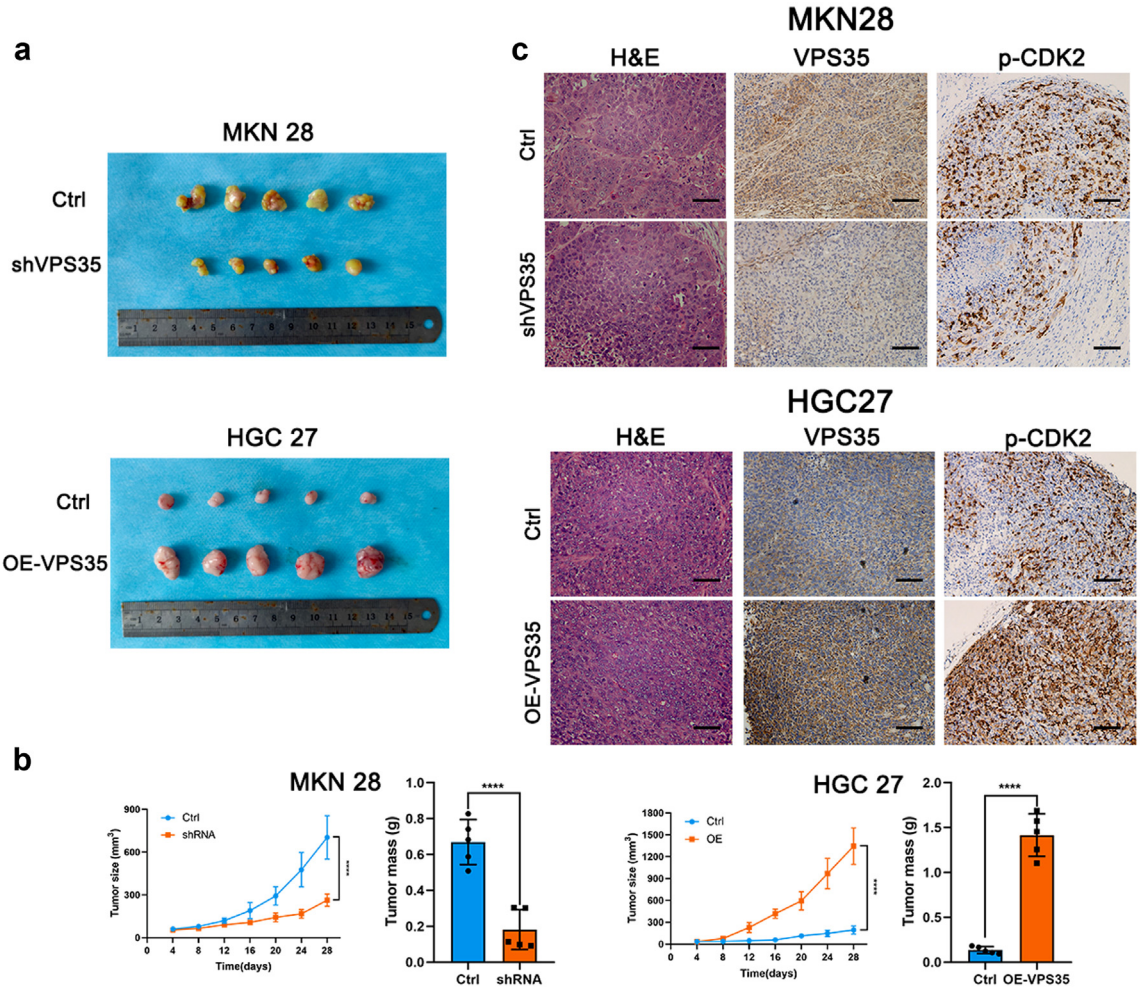

***Fig. 3:* VPS35 promoted gastric cancer development in vivo.** (a) Images of subcutaneous tumours formed by MKN28/Ctrl, MKN28/shVPS35, HGC27/Ctrl, and HGC27/VPS35 cells (five biological replicates). (b) Quantification (tumour volume at indicated time points, tumour weight at endpoint) of subcutaneous tumours formed by MKN28/Ctrl, MKN28/shVPS35, HGC27/Ctrl, and HGC27/VPS35 cells. (c) Representative images of H&E staining and IHC (VPS35 and p-CDK2) of subcutaneous tumours formed by MKN28/Ctrl, MKN28/shVPS35, HGC27/Ctrl, and HGC27/VPS35 cells. (Scale bars: 100 μm. The student's t tests, *, $p < 0.05$; **, $p < 0.01$; ***, $p < 0.001$ and ****, $p < 0.0001$.).

value = 0.043, Fisher's exact tests) were significantly enriched (Fig. 4b). Furthermore, Gene Set Enrichment Analysis (GSEA) showed that VPS35 expression was positively correlated with growth factor receptor binding (NES = –1.57, $p < 0.001$, empirical phenotype-based permutation test) (Figs. S2c-d).

reverse transcription PCR (qRT-PCR). Experiments were conducted three times independently. (b) CCK8 assay (Two-way ANOVA). Experiments were conducted three times independently. (c) Colony formation assay. Colonies were counted in three independent experiments. (Scale bars: 1 cm) (d) Cell proliferation measured by EdU incorporation. RFP: EdU-555, Scare bars: 200 μm. Experiments were conducted three times independently. (e) Western blotting for the indicated proteins in HGC27/Ctrl, HGC27/VPS35, HS-746T/Ctrl, and HS-746T/VPS35 cells, and western blotting for the indicated proteins in AGS/Ctrl, AGS/shVPS35, MKN28/Ctrl, and MKN28/shVPS35 cells. β-tubulin was used as an internal control. Experiments were conducted three times independently. (f) Flow cytometry analysis indicated that VPS35 knockdown suppressed the G1/S transition in AGS/shVPS35 and MKN28/shVPS35 cells, and VPS35 overexpression facilitated the G1/S transition in HGC27/VPS35 and HS-746T/VPS35 cells. Populations of cells at the G1, S, and G2/M phases were shown as percentages of the whole cell population. (The results were representative samples from three independent repeats, and data were present as mean ± SD. The student's t tests, *, $p < 0.05$; **, $p < 0.01$; ***, $p < 0.001$ and ****, $p < 0.0001$.).

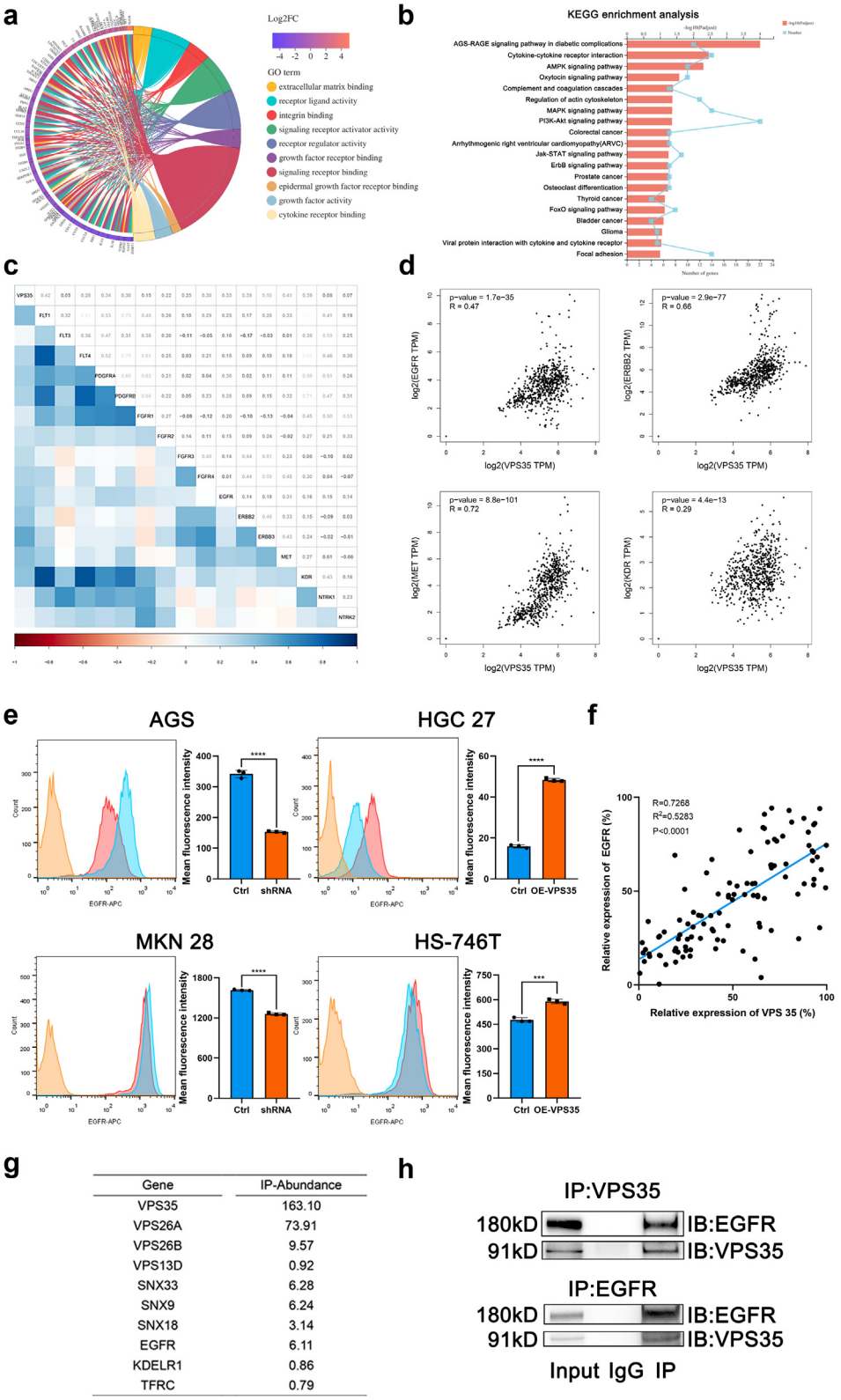

Gene	IP-Abundance
VPS35	163.10
VPS26A	73.91
VPS26B	9.57
VPS13D	0.92
SNX33	6.28
SNX9	6.24
SNX18	3.14
EGFR	6.11
KDELR1	0.86
TFRC	0.79

***Fig. 4:* Identification of VPS35 binding to EGFR.** (a) Gene Ontology pathway enrichment analysis of significantly differentially expressed genes (DEGs) between MKN28/Ctrl and MKN28/shVPS35 cells revealed by RNA-Seq. (three biological replicates, transcriptomic data were submitted to

As VPS35 plays a role in protein transportation and DEGs enriched in the MAPK pathway and receptor binding, correlation analysis between VPS35 expression levels and multiple gene expression levels of MAPK-related receptors was performed in TCGA database (Fig. 4c). We found a total of six receptor genes related to VPS35 (coefficient correlation value: $R > 0.3$), including EGFR, HER2, ERBB3, MET, VEGFR1, and VEGFR2 (Fig. 4d and S3a). As VEGFR1 was scarcely expressed in epithelial cells and ERBB3 could not convey the signal to the cell by itself, they were excluded from further validation (Fig. S3b). To confirm whether VPS35 regulates the remaining four receptors in gastric cancer cells, the density of these four receptors on the cell surface was evaluated by flow cytometry in AGS/shVPS35, MKN28/shVPS35, HGC27/VPS35, HS-746T/VPS35, and the corresponding negative control cells (Fig. 4e and S3c). We found that only EGFR density on the cell surface changed with the perturbation of VPS35 expression (Fig. 4e). The fluorescence density of EGFR on the cell surface decreased in AGS/shVPS35 and MKN28/shVPS35 cells, but increased in HGC27/VPS35 and HS-746T/VPS35 cells (Fig. 4e). IHC staining of the paired tissue microarray confirmed that VPS35 expression was positively correlated with EGFR expression in the Ruijin cohort (Fig. 4f). Immunoprecipitation and mass spectrometry (IP-MS) revealed that VPS35 binds to EGFR in the cytoplasm (Fig. 4g). Co-IP assays also confirmed that VPS35 and EGFR could bind to each other (Fig. 4h). Also, to explore whether VPS35 binds to mutated EGFR proteins, we transfected $EGFR^{L858R}$ mutated plasmids and VPS35 plasmids into HEK293T cells. Co-IP assays confirmed that VPS35 and $EGFR^{L858R}$ mutated proteins could still bind to each other (Fig. S4). Collectively, these findings indicate that VPS35 binds to EGFR, and its overexpression increases surface-EGFR density.

VPS35 recycled EGFR to the cell surface and decreased EGFR degradation

After binding to EGF and initiating downstream cascades, endocytosed EGFR localises to early endosomes, waiting to be recycled or transported to lysosomes.[14] Generally, EGFR is ubiquitinated in the endosome, recognised by ubiquitin-interacting motif-containing proteins, and targeted to lysosomes.[32] Since VPS35 is a core component of the retromer in endosomal protein trafficking, we wondered whether more VPS35 transported more EGFR back to the membrane and inhibited EGFR degradation by binding to EGFR.

Because EGFR is endocytosed into the cytoplasm after binding to EGF, sequential protein blot detection of EGFR was performed (Fig. 5a). After EGF was washed by starvation overnight, EGFR was gathered on the cell surface. With cycloheximide addition, EGFR was processed without inference of secondary protein synthesis. AGS/shVPS35 and MKN28/shVPS35 cells showed significantly lower EGFR levels 30 min after EGF addition than the corresponding negative control cells, and EGFR was nearly undetectable 60 min later (Fig. 5a). In contrast, HGC27/VPS35 and HS-746T/VPS35 cells displayed a slower rate of EGFR reduction than the negative control cells, and EGFR was still detectable at 60 min in HGC27/VPS35 and HS-746T/VPS35 cells (Fig. 5a). We also performed immunofluorescence assays at 60 and 120 min, considering their higher sensitivity when detecting sequential changes than protein blotting. AGS/shVPS35 and MKN28/shVPS35 cells showed weaker EGFR fluorescence density at every time point than the corresponding negative control cells (Fig. 5b and S5a-b). For HGC27/VPS35 and HS-746T/VPS35 cells, the mean EGFR fluorescence density was stronger at 30, 60, and 120 min than that of HGC27/Ctrl and HS-746T/Ctrl cells (Fig. 5b and Fig. S5c-d).

A cell-surface biotinylation assay was used to examine EGFR recycling.[22] Protein blot detection of biotin-tagged EGFR can reflect unrecycled EGFR. We found more biotin-EGFR in AGS/shVPS35 and MKN28/shVPS35 cells than in the control groups, indicating that fewer EGFR molecules were recycled to the surface. Meanwhile, biotin-EGFR decreased more rapidly at 30–45 min in HGC27/VPS35 and HS-746T/VPS35 cells than in the negative control cells, implying a faster rate of EGFR recycling in VPS35 overexpressed cells (Fig. 5c). Overall, these findings indicated that VPS35 slowed EGFR degradation by promoting its recycling to the cell surface.

the GEO database (GSE210320). (b) KEGG pathway enrichment analysis of significantly DEGs (Fisher's exact tests). (c) A pairwise correlation of RNA expression of VPS35 with MAPK-associated genes of receptor components (i.e., EGFR, VEGFR2, MET, and FGFR3) from TCGA gastric cancer cohort. Left triangle: a colour plot for the expression of two molecules showing different correlation by colours; diagonal: the name for each molecule; and right triangle: correlation coefficient. (d) Correlation of RNA expression of VPS35 with several related genes from the GEPIA gastric cancer cohort (Spearman's correlation). (e) Flow cytometry analysis for AGS/Ctrl, AGS/shVPS35, MKN28/Ctrl, MKN28/shVPS35, HGC27/Ctrl, HGC27/VPS35, HS-746T/Ctrl, and HS-746T/VPS35 cells. Compared with cells in the control groups, AGS/shVPS35 and MKN28/shVPS35 cells had a significantly decreased EGFR fluorescence density (left two panels), while HGC27/VPS35 and HS-746T/VPS35 cells had a significantly increased EGFR fluorescence density (right two panels). Experiments were conducted three times independently. (f) Correlation of EGFR and VPS35 expression levels by linking IHC scores of EGFR to VPS35 in paired patient samples (Pearson's correlation). (g) Different binding proteins derived from immunoprecipitation and mass spectrometry (IP-MS) of MKN28 cells. (h) Interaction of VPS35 with EGFR determined by co-Immunoprecipitation (Co-IP) assays in MKN28 cells. (The student's t tests, *, $p < 0.05$; **, $p < 0.01$; ***, $p < 0.001$ and ****, $p < 0.0001$.).

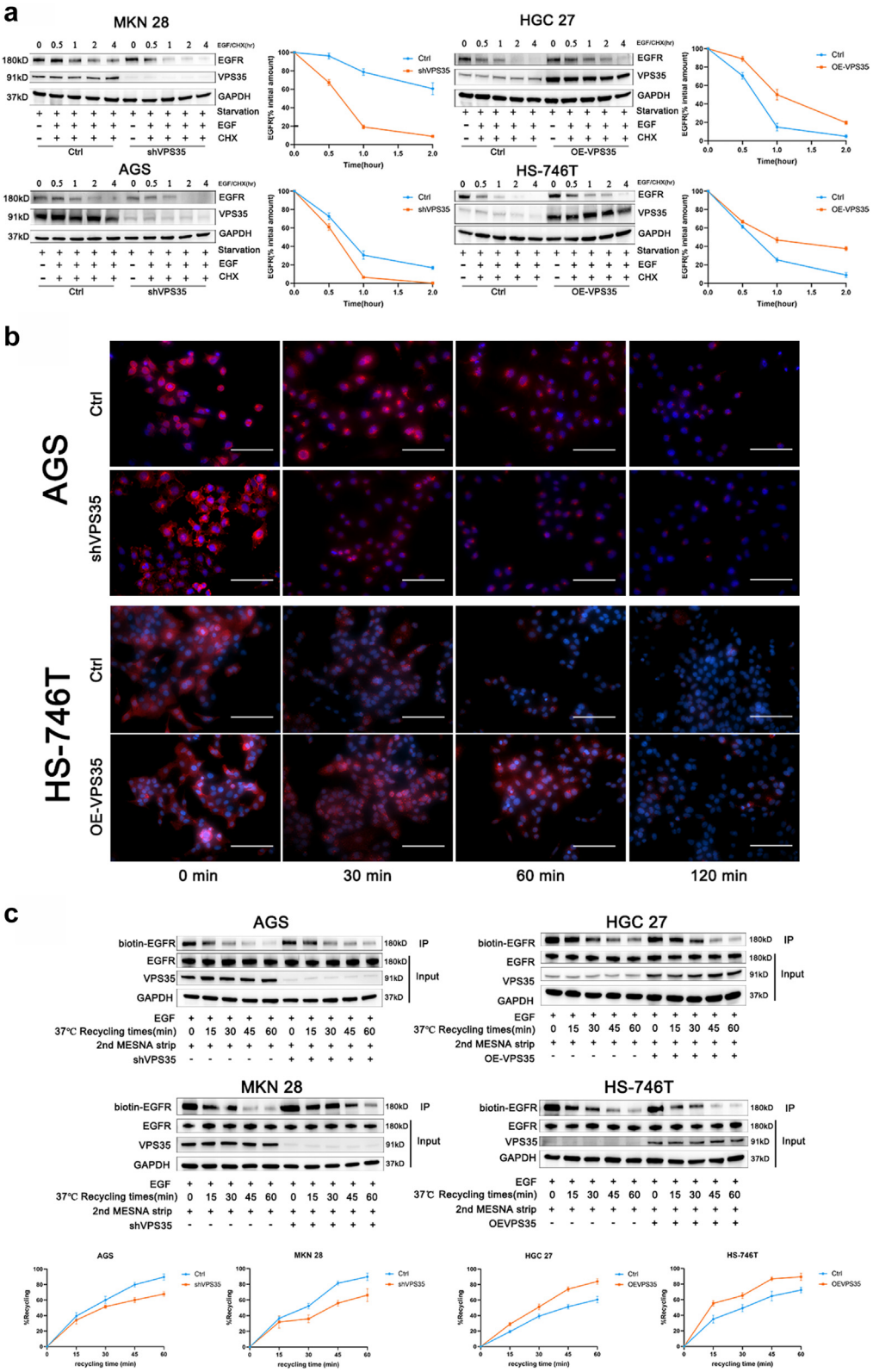

Fig. 5: **VPS35 recycled EGFR to the cell surface and decreased EGFR degradation.** (a) VPS35 knockdown enhanced EGF-induced EGFR degradation, whereas VPS35 overexpression inhibited EGFR degradation. Western blotting detected the alterations in the total EGFR

VPS35 activated EGFR downstream pathways to increase tumour growth

EGFR transmits extracellular signals mainly by activating the downstream ERK1/2 and AKT pathways. We previously found that VPS35 expression correlated with the MAPK and AKT signalling pathways using RNA-Seq analysis. Indeed, the phosphorylation level of p42/44 MAPK (known as ERK1/2) at Thr202 and Tyr204 decreased in AGS/shVPS35 and MKN28/shVPS35 cells, whereas the opposite change was found in HGC27/VPS35 and HS-746T/VPS35 cells, indicating that the ratio of p-ERK1/2 to ERK1/2 was positively related to the VPS35 expression level (Fig. 6a). We also found that the phosphorylation level of AKT decreased in AGS/shVPS35 and MKN28/shVPS35 cells, but increased in HGC27/VPS35 and HS-746T/VPS35 cells (Fig. 6a). In addition, there were more p-ERK1/2- and EGFR-negative cells in MKN28/shVPS35 tumours than in MKN28/Ctrl tumours (Fig. S6a), and HGC27/VPS35 tumours had more p-ERK1/2- and EGFR-positively stained cells than HGC27/Ctrl tumours (Fig. S6b). These results indicate that VPS35 activates EGFR downstream of the ERK1/2 and AKT pathways.

Furthermore, HGC27/VPS35 and HS-746T/VPS35 cells immersed in 200 ng/mL rhEGF proliferated more rapidly than those in 100 ng/mL rhEGF, implying an EGF-saturated concentration of over 100 ng/mL (Fig. 6b). However, the proliferation rates of HGC27/Ctrl and HS-746T/Ctrl cells with 200 ng/mL rhEGF did not exceed those with 100 ng/mL rhEGF, indicating that HGC27/VPS35 and HS-746T/VPS35 cells had a higher EGF-saturated concentration than the negative control cells (Fig. 6b and S7a). The results of the colony formation assay for HGC27/VPS35 and HS-746T/VPS35 cells were consistent with these findings (Fig. 6c). Cetuximab (an antibody blocking the extracellular domain of EGFR) was used for rescue experiments. Increasing cetuximab concentration reduced the growth difference between VPS35 overexpression cells and negative control cells. Extremely high concentrations of cetuximab (400 μg/mL) blocked surface EGFR and eliminated the difference between VPS35 overexpression cells and the negative control cells. These results indicated that EGF signals transmitted by surface EGFR in HGC27/VPS35 and HS-746T/VPS35 cells could be completely counteracted by cetuximab (Fig. 6d and e, and S7b). The results were validated by a colony formation assay, which also showed that VPS35 overexpression did not promote cell proliferation with 400 μg/mL cetuximab (Fig. 6f). These findings suggest that increased EGF signals were transmitted to the cytoplasm due to VPS35 upregulation and more EGFR on the cell surface, leading to cell proliferation. Besides of direct blocking EGFR with cetuximab, we also knockdown EGFR expression in VPS35 overexpressed cells and monitored cell growth. In our results, shEGFR-HS746T cells grew slower than Ctrl-HS746T cells, OEVPS35-HS746T cells grew faster than Ctrl-HS746T cells, and shEGFR-OEVPS35-HS746T cells grew significantly slower than both Ctrl-HS746T cells and OEVPS35-HS746T cells (Fig. S8). Similar results were shown in HGC27 cells. Our results showed that after EGFR knockdown, VPS35 upregulation could not promote cancer cell growth any more.

VPS35 sensitised gastric cancer cells to EGFR inhibitors

Interestingly, as the inhibitory effect of cetuximab on cell proliferation depended on its concentration, we also found that VPS35 affected the sensitivity of cells to cetuximab. The IC_{50} values of HGC27/VPS35 and HS-746T/VPS35 cells for cetuximab were lower than those of the negative control cells, indicating that VPS35 upregulation increases the sensitivity of cells to cetuximab (Fig. S9). As there are two main species of EGFR inhibitors, anti-EGFR monoclonal antibodies (cetuximab) and small-molecule tyrosine kinase inhibitors (erlotinib),[33] we also tested erlotinib sensitivity in VPS35-overexpressed cells. Consistent with the above findings, VPS35 overexpression decreased the IC_{50} values, whereas VPS35 knockdown increased them (Fig. 7a). Additionally, the conjoint analysis of the Genomics of Drug Sensitivity in Cancer (GDSC),[34] Cancer Cell Line Encyclopedia (CCLE),[35] and genome CRISPR–Cas9 screens also showed that VPS35 was a differentially expressed gene between the low- and high-erlotinib-sensitive groups and a prognostic gene associated with poor survival in gastric cancer specifically (Fig. S10).

We used patient-derived organoids (PDOs) to further confirm that VPS35 increases the sensitivity of gastric cancer to erlotinib. Tumours from Patient-2 (P2) had low expression levels of VPS35, whereas tumours from Patient-5 (P5) had high expression levels of VPS35

degradation in indicated cells in response to EGF stimulation in the presence of cycloheximide (left panels). Densitometric analysis of EGFR blots from three independent experiments are shown as mean ± SD (right panels). Experiments were conducted three times independently. (b) Localisation analysis of EGFR after EGF and cycloheximide treatment at different time points. At 0 min, EGFR was located mainly on the cell surface in all indicated cells after overnight starvation. With the passing of time, AGS/shVPS35 cells showed weaker fluorescence intensity compared to AGS/Ctrl cells, while HS-746T/VPS35 cells retained stronger fluorescence intensity than cells in the control group did. RFP: EGFR. Experiments were conducted three times independently. (c) VPS35 knockdown inhibited EGFR recycling and VPS35 overexpression promoted EGFR recycling. Indicated cell surfaces were labelled with Sulfo–NHS–SS-biotin on ice and stimulated for 30 min with EGF at 37 °C. Recycling of EGFR was determined at different time points indicated in the graphs by western blotting (upper panels). The values in western blotting were mean ± SD from three independent experiments (lower panels). Experiments were conducted three times independently. (Scale bars: 100 μm).

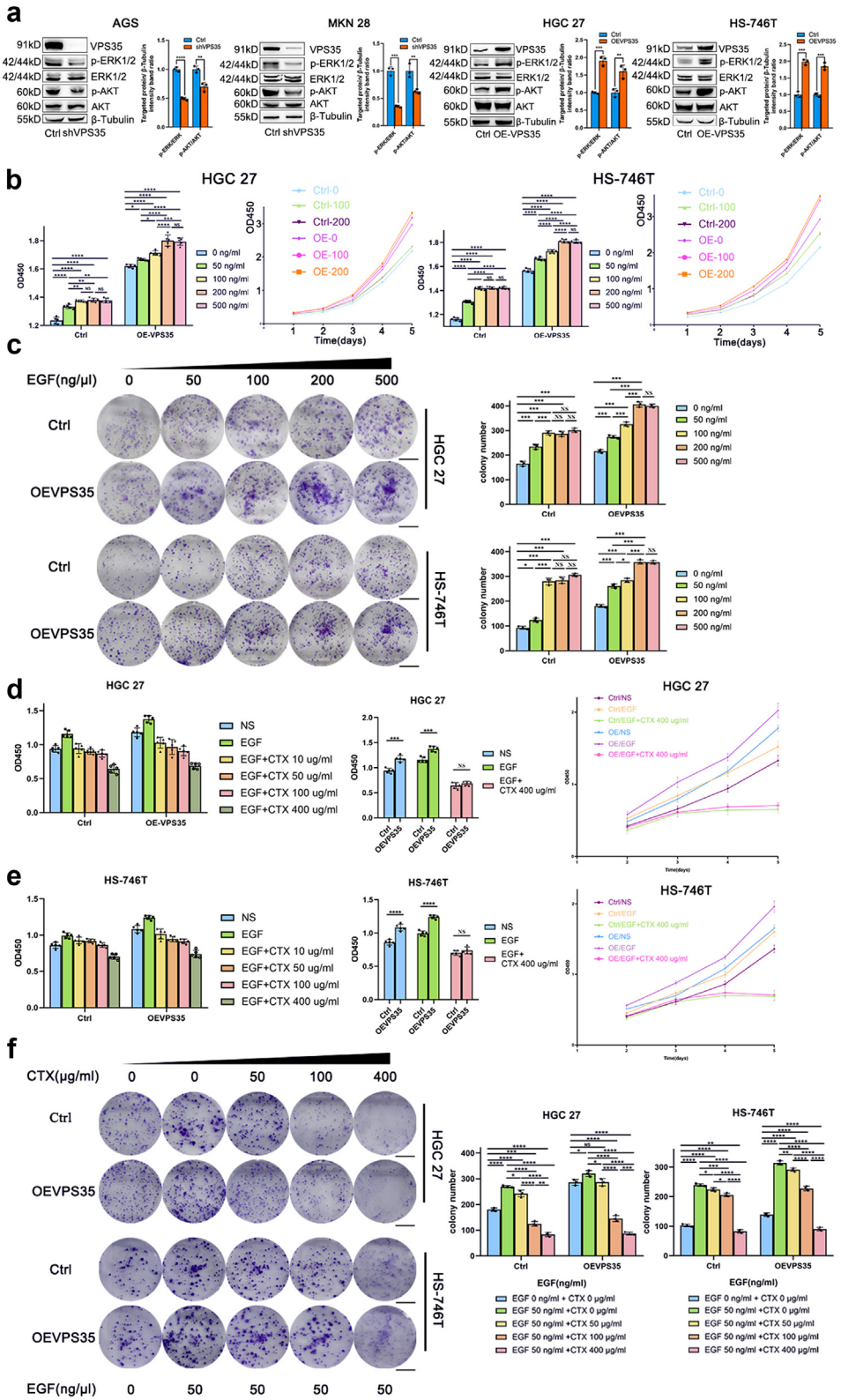

Fig. 6: **VPS35 activated EGFR downstream pathways and exerted its proliferation-promoting role via EGFR.** (a) Reduced phosphorylation levels of ERK1/2 and AKT in AGS/shVPS35 and MKN28/shVPS35 cells and increased phosphorylation levels of ERK1/2 and AKT in HGC27/VPS35

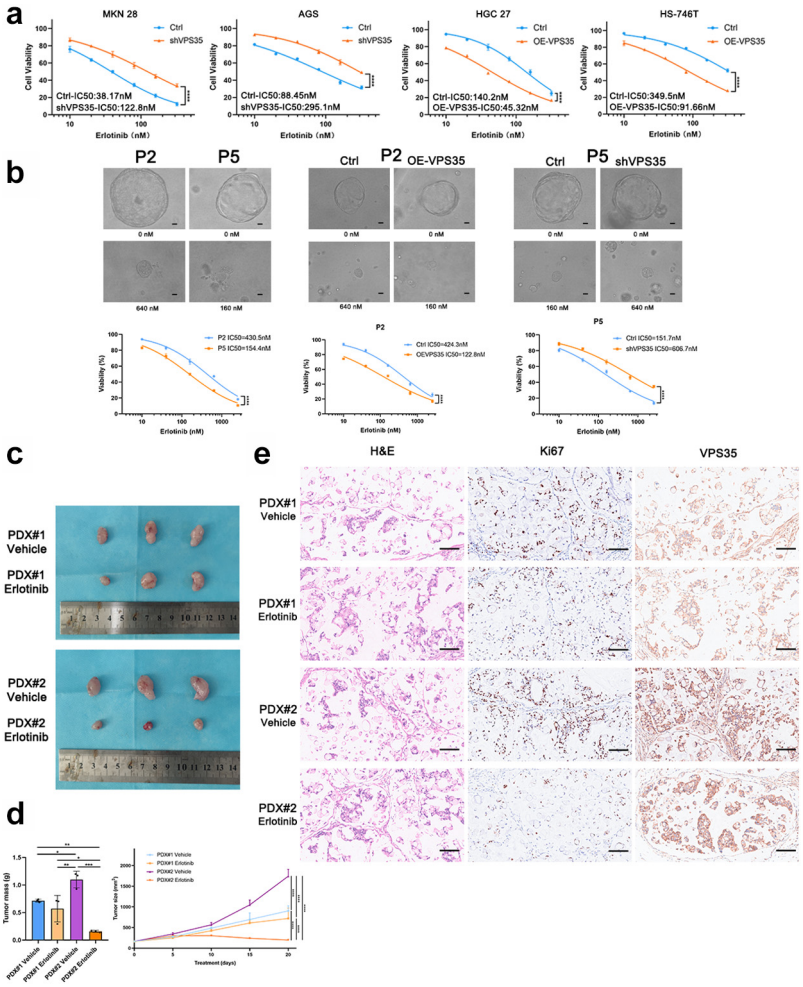

***Fig. 7:* VPS35 overexpression sensitised gastric cancer cells to erlotinib.** (a) Dose-effect curves and IC_{50} values of different erlotinib treatment groups in indicated cell lines for ten days (Extra sum-of-squares F test). Experiments were conducted three times independently. (b) Images of organoids in the vehicle- and erlotinib-treated groups treated with the indicated concentrations, and dose–effect curves with IC_{50} values of organoids with or without lentivirus transfection for ten days (Extra sum-of-squares F test). Experiments were conducted three times independently. (c) and (d) Images and quantification (tumour volume at indicated time points, tumour weight at endpoint) of subcutaneous PDX tumours with vehicle and erlotinib (Three biological replicates, Left: two-way ANOVA; right: one-way ANOVA). (e) Representative images of H&E staining and IHC (VPS35 and Ki67) of subcutaneous PDX tumours with vehicle and erlotinib treatment. (n = 3; scale bars: 100 μm, *, $p < 0.05$; **, $p < 0.01$; ***, $p < 0.001$ and ****, $p < 0.0001$.).

(Fig. S11a). P2 organoids had fewer Ki67-positive cells than P5 organoids did (Fig. S11a). Consistent with the results based on the cell lines, P5 organoids (IC_{50} = 154.4 nM) were more sensitive to erlotinib than P2 organoids (IC_{50} = 430.5 nM) (Fig. 7b). VPS35 expression was knocked down in P5 organoids (P5-KD) and ectopically overexpressed in P2 organoids (P2-OE). Frozen sections were stained by an EGFR antibody. P2-

and HS-746T/VPS35 cells (the student's t tests). Experiments were conducted three times independently. (b) CCK8 assay of HGC27/Ctrl, HGC27/VPS35, HS-746T/Ctrl, and HS-746T/VPS35 cells with the addition of EGF concentration gradients at Day 4. Experiments were conducted three times independently. (c) Colony formation assay of HGC27/Ctrl, HGC27/VPS35, HS-746T/Ctrl, and HS-746T/VPS35 cells with the addition of EGF with concentration gradients at Day 4. Colonies were counted in three independent experiments. (Scale bars: 1 cm). (d) and (e) CCK8 assay of HGC27/Ctrl, HGC27/VPS35, HS-746T/Ctrl, and HS-746T/VPS35 cells with the addition of fixed EGF and cetuximab with concentration gradients at Day 4 (Medium: the student's t tests). Experiments were conducted three times independently. EGF was used at 50 ng/mL. (f) Colony formation assay of HGC27/Ctrl, HGC27/VPS35, HS-746T/Ctrl, and HS-746T/VPS35 cells with the addition of fixed EGF and cetuximab with concentration gradients. CTX: Cetuximab. Colonies were counted in three independent experiments. (Scale bars: 1 cm. One-way ANOVA, *, $p < 0.05$; **, $p < 0.01$; ***, $p < 0.001$ and ****, $p < 0.0001$.).

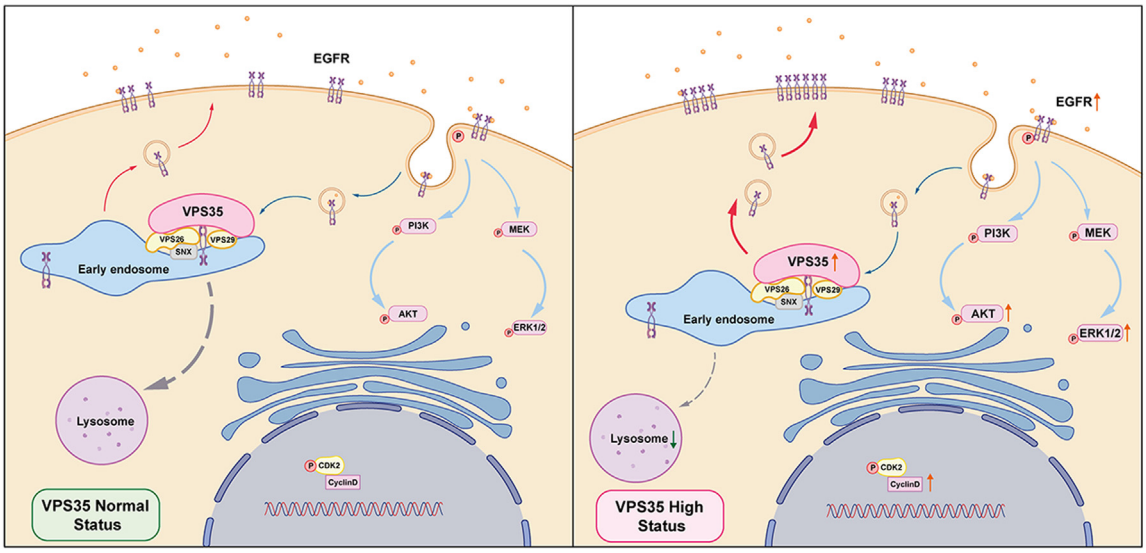

Fig. 8: **A proposed model depicts how VPS35 participates in the trafficking of EGFR and its effects on downstream ERK and AKT signalling**.

OE organoids showed stronger fluorescence intensity than P2 control organoids, whereas P5-KD organoids displayed weaker fluorescence intensity than P5 control organoids, further demonstrating that VPS35 modulated EGFR expression (Fig. S11b). Erlotinib inhibited P2-OE organoid viability (IC_{50} = 122.8 nM) more efficiently than P2 control organoids (IC_{50} = 424.3 nM), whereas P5-KD organoids (IC_{50} = 606.7 nM) were less sensitive to erlotinib than P5 control organoids (IC_{50} = 151.7 nM), as indicated by the different IC_{50} values (Fig. 7b). Thus, these findings indicate that VPS35 overexpression sensitises both gastric cancer cell lines and organoids to erlotinib, and VPS35 levels might help guide clinical erlotinib application.

We generated PDX tumors with vehicle or erlotinib. Erlotinib significantly reduced tumour growth in high-VPS35 PDX#2 group, while it did not inhibit tumour growth in low-VPS35 PDX#1 group (Fig. 7c). Moreover, erlotinib-treated PDX#2 tumours became smaller than vehicle tumours, whereas no significant difference was between erlotinib-treated and vehicle PDX#1 tumours (Fig. 7c and d). IHC staining also revealed fewer Ki67-positive cells in PDX#2 tumours than in PDX#1 tumours with erlotinib (Fig. 7e). We also generated cell-derived xenografts with peritumour injection of erlotinib (20 mg/kg, every two days) 7 days post-cell-inoculation. The results were consistent with our findings in PDX tumors (Fig. S11c-e). These findings indicate that VPS35 plays an oncogenic role in preclinical models of gastric cancer and elevates sensitivity to erlotinib.

Discussion

The retromer is a canonical complex that transports proteins between cellular compartments. VPS35 is the core component of the retromer complex. For decades, many studies have focused on the relationship between VPS35 and neurodegenerative diseases, such as Parkinson's and Alzheimer's diseases.[10,36] Recently, researchers have focused on the role of VPS35 in cancer.[11,37] For example, VPS35 is upregulated in breast cancer and promotes cell proliferation by affecting autophagy.[37] VPS35 can also promote hepatoma cell proliferation through the AKT pathway, mainly by influencing FGFR3 trafficking.[11] In this study, we investigated the role of VPS35 in gastric cancer. We found that VPS35 promoted cell proliferation, cell cycle transition, and xenograft tumour growth. Mechanistically, VPS35 overexpression increased EGFR density on the cell surface by selectively binding to endocytosed EGFR in early endosomes, recycling it back to the cell surface, decreasing EGFR degradation, and activating the downstream ERK and AKT pathways, further promoting cancer development and leading to erlotinib sensitivity (Fig. 8).

EGFR, a transmembrane protein, can activate signalling cascades, including the ERK and AKT pathways, with phosphorylated cytoplasmic residues.[16,38] After binding to its ligands, EGFR is endocytosed into early endosomes. Within the endosome, different membrane compartments hold multiple protein machineries that control cargo recycling and sorting into multivesicular bodies. Retromer and retriever

complexes take centre stage in cargo recycling.[39] Some EGFR proteins in endosomes are recycled to the cell surface by intracellular transportation, and others in multivesicular bodies are directed to lysosomes for hydrolysis.[14] Previous studies have found that EGFR recycling can take place via multiple routes, including through the calcium-modulating cyclophilin ligand[40] and adaptor protein Eps15,[41] showing that cells can increase EGFR efficiency in various ways. In normal cells, a delicate equilibrium between EGFR recycling and degradation sustains moderate signalling, and aberrations in either route would cause dysregulated cell proliferation and oncogenesis.[14,33] We demonstrated that VPS35 transported endocytosed EGFR back to the cell surface, increased EGFR density, and activated the downstream ERK and AKT pathways, through which VPS35 exerts its oncogenic function in gastric cancer. This discovery indicated that the EGFR recycling routes were replenished in the cytoplasm, which is a newly discovered retromer function in EGFR recycling, and illustrated the mechanism of VPS35-mediated recycling in cancer development.

Gastric cancer responds poorly to immunotherapy and molecular-targeted therapy[3] such as EGFR inhibitors. It has been proposed that the failure of anti-EGFR therapy results from the enrolment of patients without prior genomic detection and selection.[12] Recently, Maron et al. reported the clinical response of eight EGFR-amplified patients; complete response was observed in 43% (3/7) of patients and partial response in one patient.[12] Ji et al. also reported a GC subtype with EGFR amplification and overexpression benefit from anti-EGFR therapy.[42] Recycling EGFR serves as an economical way to upregulate EGFR.[14] In our study, VPS35 recycled the endocytosed EGFR to the cell surface. Interestingly, we observed that VPS35 could elevate the sensitivities of gastric cancer cells to both species of EGFR inhibitors, cetuximab and erlotinib. Additionally, VPS35 increased the sensitivity of gastric cancer organoids to erlotinib.

In our study, VPS35 was negatively correlated with G protein-coupled receptor and phospholipase C upregulation (Fig. S12). Indeed, stimulatory G-protein alpha subunits are also thought to participate in the poor response to anti-EGFR therapy.[12] The effects of EGFR accumulation and GPCR inhibition indicated that VPS35 might serve as a more comprehensive indicator than EGFR expression for anti-EGFR therapy in gastric cancer, similar to the KRAS status which indicates EGFR inhibitor efficacy in colorectal cancer.[43] Our study is rather preliminary, showing the link between VPS35 and anti-EGFR drugs. Using only one shRNA could not exclude off-target possibility, which is our limitation. There is still a long way to go with clinical trials, like retrospective study and prospective cohort study to reveal the relation between VPS35 and anti-EGFR drugs in the real world. Further research is recommended to investigate the impact of VPS35 in all aspects of anti-EGFR therapy.

In conclusion, our study sheds new light on the ERK/AKT pathway-activated and tumourigenic role of VPS35 in gastric cancer. Mechanistically, this study showed that VPS35 promotes EGFR recycling to the cell surface, which may amplify the network of intracellular protein transportation and receptor trafficking. As VPS35 increases the sensitivity of gastric cancer to EGFR inhibitors, VPS35 could be a potential treatment effect marker to stratify patients for anti-EGFR therapy in gastric cancer.

Contributors

Bingya Liu and Jianfang Li: conceptualization, supervision and writing-review & editing.

Junxian Yu: investigation, data duration and writing-original draft.

Haoran Feng: investigation, data verification and writing-original draft.

Qingqing Sang: investigation and software.

Fangyuan Li, Xiongyan Wu and Junyi Hou: formal analysis.

Mengdi Chen: data verification and writing-review & editing.

Tao Pan: validation.

Chao Yan and Zhenggang Zhu: resources.

Zhuoqing Xu, Beiqin Yu, Liping Su: methodology.

All authors read and approved the final version of the manuscript.

Data sharing statement

The dataset generated by RNA-Seq is available in the Gene Expression Omnibus public database under data series accession number GSE210320.

Declaration of interests

All the authors have declared no conflicts of interests.

Acknowledgements

This research was supported by grants from the National Natural Science Foundation of China (No. 81772509 and No. 82072605 to BY Liu, No. 81871904 to ZG Zhu, No. 81871902 and No. 82072616 to LP Su, No. 82003169 to HR Feng, and No. 81902393 to BQ Yu), and the Natural Science Foundation of Shanghai (No. 19ZR1431700 to BQ Yu).

Appendix A. Supplementary data

Supplementary data related to this article can be found at https://doi.org/10.1016/j.ebiom.2023.104451.

References

1 Sung H, Ferlay J, Siegel RL, et al. Global cancer statistics 2020: GLOBOCAN estimates of incidence and mortality worldwide for 36 cancers in 185 countries. *CA Cancer J Clin*. 2021;71:209–249.
2 Siegel RL, Miller KD, Fuchs HE, Jemal A. Cancer statistics, 2021. *CA Cancer J Clin*. 2021;71:7–33.
3 Joshi SS, Badgwell BD. Current treatment and recent progress in gastric cancer. *CA A Cancer J Clin*. 2021;71:264–279.
4 Fukuoka S, Hara H, Takahashi N, et al. Regorafenib plus nivolumab in patients with advanced gastric or colorectal cancer: an open-label, dose-escalation, and dose-expansion phase Ib trial (REGONIVO, EPOC1603). *J Clin Oncol*. 2020;38:2053–2061.
5 Behan FM, Iorio F, Picco G, et al. Prioritization of cancer therapeutic targets using CRISPR-Cas9 screens. *Nature*. 2019;568:511–516.
6 Li F, Li J, Yu J, et al. Identification of ARGLU1 as a potential therapeutic target for gastric cancer based on genome-wide functional screening data. *eBioMedicine*. 2021;69:103436.
7 Hierro A, Rojas AL, Rojas R, et al. Functional architecture of the retromer cargo-recognition complex. *Nature*. 2007;449:1063–1067.

8 Bonifacino JS, Rojas R. Retrograde transport from endosomes to the trans-Golgi network. *Nat Rev Mol Cell Biol*. 2006;7:568–579.
9 Carosi JM, Hein LK, van den Hurk M, et al. Retromer regulates the lysosomal clearance of MAPT/tau. *Autophagy*. 2021;17:2217–2237.
10 Ding Y, Li Y, Chhetri G, et al. Parkinson's disease causative mutation in Vps35 disturbs tetherin trafficking to cell surfaces and facilitates virus spread. *Cells*. 2021;10.
11 Zhang G, Tang X, Liang L, et al. DNA and RNA sequencing identified a novel oncogene VPS35 in liver hepatocellular carcinoma. *Oncogene*. 2020;39:3229–3244.
12 Maron SB, Alpert L, Kwak HA, et al. Targeted therapies for targeted populations: anti-EGFR treatment for EGFR-amplified gastroesophageal adenocarcinoma. *Cancer Discov*. 2018;8:696–713.
13 Nicholson RI, Gee JM, Harper ME. EGFR and cancer prognosis. *Eur J Cancer*. 2001;37:S9–S15.
14 Tomas A, Futter CE, Eden ER. EGF receptor trafficking: consequences for signaling and cancer. *Trends Cell Biol*. 2014;24:26–34.
15 Schenck A, Goto-Silva L, Collinet C, et al. The endosomal protein Appl1 mediates Akt substrate specificity and cell survival in vertebrate development. *Cell*. 2008;133:486–497.
16 Citri A, Yarden Y. EGF-ERBB signalling: towards the systems level. *Nat Rev Mol Cell Biol*. 2006;7:505–516.
17 Kim D, Langmead B, Salzberg SL. HISAT: a fast spliced aligner with low memory requirements. *Nat Methods*. 2015;12:357–360.
18 Pertea M, Pertea GM, Antonescu CM, Chang TC, Mendell JT, Salzberg SL. StringTie enables improved reconstruction of a transcriptome from RNA-seq reads. *Nat Biotechnol*. 2015;33:290–295.
19 Li B, Dewey CN. RSEM: accurate transcript quantification from RNA-Seq data with or without a reference genome. *BMC Bioinf*. 2011;12:323.
20 Love MI, Huber W, Anders S. Moderated estimation of fold change and dispersion for RNA-seq data with DESeq2. *Genome Biol*. 2014;15:550.
21 Xie C, Mao X, Huang J, et al. KOBAS 2.0: a web server for annotation and identification of enriched pathways and diseases. *Nucleic Acids Res*. 2011;39:W316–W322.
22 Ye QH, Zhu WW, Zhang JB, et al. GOLM1 modulates EGFR/RTK cell-surface recycling to drive hepatocellular carcinoma metastasis. *Cancer Cell*. 2016;30:444–458.
23 Driskell OJ, Mironov A, Allan VJ, Woodman PG. Dynein is required for receptor sorting and the morphogenesis of early endosomes. *Nat Cell Biol*. 2007;9:113–120.
24 Liu H, Paddock MN, Wang H, et al. The INPP4B tumor suppressor modulates EGFR trafficking and promotes triple-negative breast cancer. *Cancer Discov*. 2020;10:1226–1239.
25 Xu Z, Gao H, Zhang Y, et al. CCL7 and TGF-β secreted by MSCs play opposite roles in regulating CRC metastasis in a KLF5/CXCL5-dependent manner. *Mol Ther*. 2022;30(6):2327–2341.
26 Nishimura N, Sasaki T. Cell-surface biotinylation to study endocytosis and recycling of occludin. *Methods Mol Biol*. 2008;440:89–96.
27 Caswell PT, Chan M, Lindsay AJ, McCaffrey MW, Boettiger D, Norman JC. Rab-coupling protein coordinates recycling of alpha5-beta1 integrin and EGFR1 to promote cell migration in 3D microenvironments. *J Cell Biol*. 2008;183:143–155.
28 Xu Z, Zhu C, Chen C, et al. CCL19 suppresses angiogenesis through promoting miR-206 and inhibiting Met/ERK/Elk-1/HIF-1alpha/VEGF-A pathway in colorectal cancer. *Cell Death Dis*. 2018;9:974.
29 Weichert W, Röske A, Gekeler V, et al. Association of patterns of class I histone deacetylase expression with patient prognosis in gastric cancer: a retrospective analysis. *Lancet Oncol*. 2008;9:139–148.
30 Corso S, Isella C, Bellomo SE, et al. A comprehensive PDX gastric cancer collection captures cancer cell-intrinsic transcriptional MSI traits. *Cancer Res*. 2019;79:5884–5896.
31 Ajani JA, Xu Y, Huo L, et al. YAP1 mediates gastric adenocarcinoma peritoneal metastases that are attenuated by YAP1 inhibition. *Gut*. 2021;70:55–66.
32 Clague MJ, Liu H, Urbé S. Governance of endocytic trafficking and signaling by reversible ubiquitylation. *Dev Cell*. 2012;23:457–467.
33 Ciardiello F, Tortora G. EGFR antagonists in cancer treatment. *N Engl J Med*. 2008;358:1160–1174.
34 Iorio F, Knijnenburg TA, Vis DJ, et al. A landscape of pharmacogenomic interactions in cancer. *Cell*. 2016;166:740–754.
35 Ghandi M, Huang FW, Jané-Valbuena J, et al. Next-generation characterization of the cancer cell line Encyclopedia. *Nature*. 2019;569:503–508.
36 Vagnozzi AN, Li JG, Chiu J, et al. VPS35 regulates tau phosphorylation and neuropathology in tauopathy. *Mol Psychiatr*. 2021;26:6992–7005.
37 Li X, Cao Y, Yu X, Jin F, Li Y. A novel autophagy-related genes prognostic risk model and validation of autophagy-related oncogene VPS35 in breast cancer. *Cancer Cell Int*. 2021;21:265.
38 Chong CR, Jänne PA. The quest to overcome resistance to EGFR-targeted therapies in cancer. *Nat Med*. 2013;19:1389–1400.
39 Chen KE, Healy MD, Collins BM. Towards a molecular understanding of endosomal trafficking by Retromer and Retriever. *Traffic*. 2019;20:465–478.
40 Tran DD, Russell HR, Sutor SL, van Deursen J, Bram RJ. CAML is required for efficient EGF receptor recycling. *Dev Cell*. 2003;5:245–256.
41 Chi S, Cao H, Wang Y, McNiven MA. Recycling of the epidermal growth factor receptor is mediated by a novel form of the clathrin adaptor protein Eps15. *J Biol Chem*. 2011;286:35196–35208.
42 Zhang L, Yang J, Cai J, et al. A subset of gastric cancers with EGFR amplification and overexpression respond to cetuximab therapy. *Sci Rep*. 2013;3:2992.
43 Adelstein BA, Dobbins TA, Harris CA, Marschner IC, Ward RL. A systematic review and meta-analysis of KRAS status as the determinant of response to anti-EGFR antibodies and the impact of partner chemotherapy in metastatic colorectal cancer. *Eur J Cancer*. 2011;47:1343–1354.